Molecular Type Permutation Shift Keying in Molecular MIMO Communications for IoBNT

Yuankun Tang, Yu Huang, Chan-Byoung Chae, *Fellow, IEEE*, Wei Duan, *Member, IEEE*, Miaowen Wen, *Senior Member, IEEE*, and Lie-Liang Yang, *Fellow, IEEE*

***Abstract*—Molecular communication (MC) is a bio-inspired communication paradigm, which lays the foundation for the Internet of Bio-NanoThings (IoBNT) in the medical field. As a high energy-efficient information transfer method, MC via diffusion (MCvD) is envisioned as a promising candidate for IoBNT but suffers from low date rates due to the long tail of the channel impulse response (CIR). To this end, the multiple-input multiple-output (MIMO) technique has been introduced to MCvD. However, the inter-symbol interference (ISI) and inter-link interference (ILI) deteriorate the bit error rate (BER) performance of MIMO MCvD systems. In this paper, molecular type permutation shift keying in the space domain (MTPSK-SD) and time-interleaved MTPSK-SD are proposed for MIMO MCvD systems to improve the BER performance by reducing ILI. The principle of MTPSK-SD is further generalized to the spatio-temporal domain, yielding three spatio-temporal modulation schemes, which can provide desirable BER performance without requiring any CIR information in the communication scenarios affected by different levels of ISI and ILI. Two low-complexity detectors are proposed to obtain different trade-offs between anti-ILI and anti-ISI performance. Furthermore, a complementary coding scheme, which can effectively reduce the ILI under the considered symmetrical system topology, is designed and applied to all the proposed modulation schemes. Additionally, the BER upper bound is analyzed. Numerical simulations on BER corroborate the analysis and show that the proposed schemes are promising multi-molecule modulation alternatives, which outperform the existing MIMO MCvD modulation schemes.**

***Index Terms*—Molecular communication, nanonetworks, modulation, inter-link interference, inter-symbol interference, MIMO.**

The work was supported in part by the National Natural Science Foundation of China under Grant 61871190 and Grant 61801249, in part by the Natural Science Foundation of Guangdong Province under Grant 2018B030306005, in part by the Pearl River Nova Program of Guangzhou under Grant 201806010171, and in part by the Fundamental Research Funds for the Central Universities under Grant 2019SJ02. (*Corresponding author: Wei Duan, Miaowen Wen.*)

This paper has been presented in part at the IEEE Wireless Communications and Networking Conference (WCNC), Nanjing, China, 2021.

Y. Tang and M. Wen are with the School of Electronics and Information, Nantong University, Nantong 226019, China, and also with the School of Electronic and Information Engineering, South China University of Technology, Guangzhou 510640, China (e-mail: eeyktang@mail.scut.edu.cn; eemwwen@scut.edu.cn).

Y. Huang is with the School of Electronic and Information Engineering, South China University of Technology, Guangzhou 510640, China (e-mail: ee06yuhuang@mail.scut.edu.cn).

C.-B. Chae is with the School of Integrated Technology, Yonsei Institute of Convergence Technology, Yonsei University, Seoul 03722, South Korea (e-mail: cbchae@yonsei.ac.kr).

W. Duan is with the School of Electronics and Information, Nantong University, Nantong 226019, China (e-mail: sinder@ntu.edu.cn).

L.-L. Yang is with the Southampton Wireless Group, School of Electronics and Computer Science, University of Southampton, Southampton SO17 1BJ, U.K. (e-mail: lly@ecs.soton.ac.uk).

I. Introduction

The unprecedented outbreak of the severe acute respiratory syndrome coronavirus, termed as COVID-19 by the World Health Organization, has posed a severe public health problem [1]. To combat the COVID-19 pandemic, a more in-depth understanding of viral transmission and detection methods is of great necessity. The viral aerosol transmission, which is regarded as one of the potential transmission routes of the COVID-19, can be studied as a molecular communication (MC) problem [2]. Despite the point-to-point MC, the devices for the viral aerosol detection are envisioned to be part of the Internet of Things (IoT) [3, 4]. Except for the macro-scale MC cases above, its micro-scale implementation underpins the emerging Internet of Bio-NanoThings (IoBNT), which is anticipated to monitor the health and detect viruses in the body based on the engineering of biological embedded computing devices [6]. In light of these applications, MC can achieve the multi-scale IoT, especially to facilitate the progress of IoT in the medical and health care fields such as targeted drug delivery [7] and disease detection [8, 9].

Molecular communication via diffusion (MCvD), which needs neither external energy supplies nor sophisticated communication infrastructure, provides a viable transmission method for MC [10]. However, since the long tail of the channel impulse response (CIR) causes serious inter-symbol interference (ISI), the MCvD channel is subject to low data rates [11]. To solve this problem, the multiple-input multiple-output (MIMO) technique, which is a well-developed technique in conventional radio-based communications [12], was first introduced to MC in [13]. Meng *et al*. proposed the spatial diversity and spatial multiplexing strategies to enhance the bit error rate (BER) performance and throughput, respectively [13]. They ignored the ISI and focused on the effect of inter-link interference (ILI) that is one of the main challenges for MIMO systems. To analytically consider the ISI and ILI, the authors in [14] proposed five detection methods, which require information of emitted molecules or CIR. For molecular MIMO prototypes, the authors in [15] built a macro-scale tabletop molecular MIMO testbed, and implemented the detection methods proposed in [14] on the prototype. Furthermore, Lee *et al.* extended the work in [15], demonstrating an in-vessel molecular MIMO communication platform, where a flow exists in the tube environment [16]. Unlike most of the prototypes with the airborne channel, an underwater MIMO-MC testbed was designed in [17], where the space shift keying (SSK) technique is validated in practice.

As for channel estimation and equalization, the authors in [18] proposed maximum-likelihood (ML) and least-squares estimation methods for diffusive MIMO systems and corresponding equalization methods to mitigate the ISI and ILI. In [19], a linear equalization framework was designed to reduce the constellation errors for MIMO systems. For spatial diversity coding techniques, repetition coding (RC) and Alamouti-type coding were studied for MIMO-MC in [20], where RC outperforms Alamouti-type coding, as the ILI for RC has a constructive effect on the intended signal strength. Wu *et al.* studied an asymmetrical molecular MIMO structure, and proposed to use a zero-forcing detection approach to mitigate the ILI [21]. In [22], enzymes were used to degrade information molecules so that they would not interfere with subsequent transmissions and neighboring communication links. The above-mentioned channel estimation and pre-coding methods can enhance performance of MIMO MCvD systems; however, they require additional information or substance to assist the symbol detection.

On the other hand, carefully designed modulation schemes are also effective in combating ISI and ILI with low energy costs [23]. To mitigate the ISI impairment in MCvD systems, the information bits can be encoded on the molecular types, pulse positions, and type permutations, corresponding to molecular shift keying [24, 25], pulse position modulation (PPM) [26], and molecular type permutation shift keying (MTPSK) [27], respectively. The recently emerging MTPSK can effectively reduce the effect of ISI by enlarging the transmission intervals of molecules with the same type [27]. Concerning the transmitter's limitations on the molecule production rate and the finite storage capacity, an adaptive release duration modulation was proposed in two cases of the absence and the presence of ISI [28]. Diverse modulation schemes were designed for MIMO MCvD systems to further combat the ILI in addition to the ISI. Spatial modulation (SM), which uses the indices of the antennas of the transmitter to convey additional information bits, was introduced to MC by Huang *et al.* in [29]. They proposed molecular space shift keying (MSSK), which only activates a single transmitter each time to avoid the ILI in the current transmitted symbol, and assumed short lengths of ILI and ISI. However, the ISI and ILI tend to be long in practical MIMO-MCvD scenarios. The authors in [30] proposed molecular spatial modulation (MSM) and quadrature (Q-)MSSK for the system having access to two types of molecules to combat the ILI and ISI, respectively. However, MSM and QMSSK may not provide a reliable transmission when both ISI and ILI are serious.

In this paper, both the ILI and ISI impacts on the MIMO MCvD channel are investigated. Furthermore, we propose four novel modulation schemes to comprehensively cope with various levels of ISI and ILI, including the harsh communication scenarios affected by the serious ILI and ISI. BER performance analysis and numerical simulations demonstrate that the proposed schemes outperform the existing modulation schemes for MIMO MCvD systems. The overall contributions of this paper include:

- We propose an MTPSK in the space domain (MTPSK-SD) that modulates information on the permutations of different molecular types emitted by nano-machines with different indices. A low-complexity detection method without requiring CIR information is proposed.
- To combat ILI, we apply a time interleaving method to MTPSK-SD (TI-MTPSK-SD), where different pairs of transceivers communicate at different time slots. We find that TI-MTPSK-SD has a desirable benefit to ILI mitigation at no cost of external hardware or calculation complexity when compared with MTPSK-SD.
- Combining MTPSK-SD with MTPSK in the time domain (TD) [27], we propose an MTPSK-SD-TD to combat both ISI and ILI. Two low-complexity detection methods are also proposed to provide different trade-offs between ILI-combating ability and ISI-combating ability.
- We design two spatio-temporal modulation schemes by combining MTPSK-SD with PPM (MTPSK-SD-PPM) and MTPSK-TD with SSK (MTPSK-TD-SSK), respectively. Our studies show that MTPSK-TD-SSK mitigates the detrimental effect of ILI, and presents the optimal BER performance when ILI is medium but ISI is serious. By contrast, MTPSK-SD-PPM exploits the constructive effect of ILI and has the optimal BER performance when MCvD systems are affected by serious ILI and ISI.
- Considering the property of ILI that an intended link is likely to suffer from the interference of its adjacent links, we design a complementary coding scheme to avoid activating the permutations prone to ILI, and to minimize the BER caused by the symbol error detection.

The remainder of this paper is organized as follows. In Section II, the system topology of MIMO MCvD and channel model affected by ISI and ILI are outlined. The modulation principles and receiver designs of the four modulation schemes are proposed in Section III, followed by the design of the complementary coding rule. In Section IV, we take MTPSK-SD-TD as an example to derive the BER upper bound. Section V provides numerical simulation results. Finally, the conclusion of this paper is drawn in Section VI, where the future work is also anticipated.

II. System Model

A. System Topology

Similar to the system topology considered in [30], an $M \times M$ MIMO systemy for MCvD within a 3-D unbounded environment is considered in this paper, as shown in Fig. 1. The system consists of a transmitter block (TX) equipped with M point-like transmit nano-machines (TNs) on its surface and a receiver block (RX) attached M passive spherical receive nano-machines (RNs). When emitting pulses of molecules towards the receiver, the TX is assumed to be capable of perfectly controlling the stored molecules of M types and the emission procedure of the TNs, according to the employed modulation scheme. The RX is assumed to be able to observe the number of molecules within each RN and distinguish different types of molecules, based on which RX detects the information bits according to the modulation employed. It is worth noting that the nano-machines on each side form a

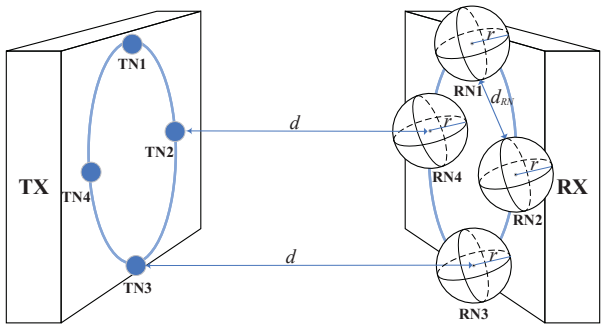

Fig. 1. Model of the 4×4 MIMO MCvD system.

uniform circular array (UCA) of nodes, which are angular-wise equally separated from the center of their corresponding nano-machines [30]. Assume that the TX-RX pair has been synchronized at symbol level based on the synchronization methods that can be exploited in MIMO systems [31, 32].

To clearly illustrate the topology structure, we exemplify a 4 × 4 MIMO MCvD system, as shown in Fig. 1. The RNs are assumed to be perfectly aligned, respectively, to their corresponding point-like TNs [30]. Under this assumption, the distances from TNs to their corresponding RNs' centers are expressed as d. The shortest distance between the surfaces of the adjacent RNs is denoted by d_{RN}. The radius of each RN equals r. Intuitively, the distances between the centers of two adjacent RNs as well as two adjacent TNs are both $d_{RN}+2r$.

B. Channel Model

Assume that the emitted molecules propagate in the channel based on the Brownian motion without flow. According to the Fick's second law of diffusion, the possibility $h_{ij}(t)$ of an information molecule, which is emitted by TN_j at $t=0$ and observed by RN_i at time t, can be expressed as [29]

$$h_{ij}(t) = \frac{1}{(4\pi Dt)^{\frac{3}{2}}} \exp\left(-\frac{d_{ij}^2}{4Dt}\right), \tag{1}$$

where d_{ij} is the distance between TN_j and the center of RN_i, and D denotes the diffusion coefficient of information molecules. Note that in this paper, all information molecules are assumed to be the isomers having the same D in the same propagation medium considered [33].

For sequent bit transmissions with a symbol duration T_s, the possibility of an information molecule observed by RN_i at the discrete instant $t=vT_s$ can be calculated by substituting $t=vT_s$ in (1). Due to the heavy tail characteristics of CIR in MCvD, the channel memory is infinite, which means that the CIR needs infinite observations to be perfectly modeled. However, for practice implementation, the CIR can be modeled by considering L symbol durations. By its nature, L also denotes the length of ISI.

Consider that information molecules can be detected in the spherical RNs with the volume of $V_r = \frac{4}{3}\pi r^3$. According to the uniform concentration assumption [34], the concentration of information molecules in RN_i is assumed to be equal to that expected at the center of RN_i. This assumption is valid, provided that the communication distance d_{ij} is sufficiently larger than the radii r of RNs and the symbol duration T_s is longer than or close to $d_{ij}^2/6D$ [34]. Consider that TN_j emits E_e molecules of a certain type, all RNs sample the number of molecules after a time interval of $t_m = d^2/6D$ from the emission instant to obtain the expected maximum of received molecules over the intended link [35]. The number of the m-th type molecules, which are emitted by TN_j at $t=vT_s$ and observed by RN_i at time $t=vT_s+t_m$, is denoted by $Z_{m,ij}(v)$, and can be expressed as

$$Z_{m,ij}(v) = \left(E_e V_r h_{ij}[0] + n_i(v)\right) s_{m,j}(v), \tag{2}$$

where $V_r h_{ij}[0]$ is the possibility of one molecule emitted by TN_j and observed by RN_i at time $t = vT_s + t_m$; $n_i(v)$ denotes the counting noise induced by the v-th emitted pulse of molecules; $s_{m,j}(v) = 1$ or 0 indicates whether TN_j emits E_e molecules of the m-th type at the v-th instant. $Z_{m,ij}(v)$ can be modeled by a binomial distribution, i.e., $Z_{m,ij}(v) \sim \mathcal{B}\big(E_e, V_r h_{ij}[0]\big)$ [36, 37]. When E_e is a large number and $V_r h_{ij}[0]$ is small, the binomial distribution can be closely approximated as a Poisson distribution $Z_{m,ij}(v) \sim \mathcal{P}\big(\lambda_{ij,0} = E_e V_r h_{ij}[0]\big)$ [38], which can be easily satisfied in common communication scenarios of MCvD.

Considering the effect of ISI and ILI, the number of molecules observed by each RN is determined by the emitted molecules from all TNs within the recent $L+1$ symbols. As shown in [39], provided that $T_s > r^2/D$, the observations in terms of the molecular numbers sampled at different instants are mutually independent. Since the sum of multiple independent Poisson random variables remains Poisson distributed, the total number of molecules of the m-th type observed by RN_i at the v-th instant can be modeled as $Z_{m,i}(v) \sim \mathcal{P}\big(\Lambda_{m,i}(v)\big)$, in which

$$\Lambda_{m,i}(v) = E_e V_r \sum_{\alpha=v-L}^{v} \sum_{j=1}^{M} s_{m,j}(\alpha) h_{ij}[v-\alpha] + \lambda_{env}, \tag{3}$$

where λ_{env} represents the Poisson parameter of the environment noise caused by the same type of molecules emitted from other MC systems, and thus λ_{env} is independent of the considered TX.

III. Modulation Principle and Receiver Design

In this section, we first introduce MTPSK-SD as a basic modulation scheme for MIMO MCvD systems. In order to combat ILI, the TI-MTPSK-SD scheme is then proposed, which introduces the time-domain interleaving so as to avoid activating all TNs at the same time. Furthermore, based on the fact that adjacent links yield the strongest ILI, we design a complementary coding scheme to increase reliability by reducing the ILI-caused symbol error detection. Next, by considering the effect of both ISI and ILI, we propose three spatio-temporal modulation schemes, namely the MTPSK-SD-TD, MTPSK-TD-SSK, and MTPSK-SD-PPM, which are designed for implementation in different MC scenarios affected by various levels of ISI and ILI. Additionally, as the nano-machines usually cannot undertake cumbersome calculation tasks, low-complexity detection methods corresponding to their modulation counterparts are proposed.

A. (TI-)MTPSK-SD and Complementary Coding Scheme

1) MTPSK-SD: Inspired by the idea that information can be transmitted by molecular type permutations on different emission instants [27], we extend the MTPSK to the MIMO-MC architecture, using the permutation pattern in the spatial domain for information encoding.

To implement MTPSK-SD, each TN emits only one out of the M types at every emission instant. The types of molecules emitted by M TNs are different from each other during the same symbol duration, and the information bits are encoded on their permutation. Since there are in total $M!$ permutation candidates, $b = \lfloor \log_2 M! \rfloor$ information bits can potentially be transmitted per symbol.

We choose $N = 2^b$ out of the $M!$ permutation candidates as activation patterns, which compose a space symbol set $\mathbf{S}^s = \{\mathbf{S}_1^s, \mathbf{S}_2^s, \ldots, \mathbf{S}_N^s\}$. It is worth noting that the selection of activation patterns from $M!$ permutation candidates and the rule of mapping information bits to the selected permutations have significant effect on the BER performance of MTPSK-SD, which will be detailed in subsection III-A-3. The activation pattern of the u-th symbol $\mathbf{S}_u^s$ is an $M \times M$ permutation matrix with only one entry equal to one in each row and column, and the rest of them are zero. The (m, j)-th entry of $\mathbf{S}_u^s$, denoted by $s_{m,j}^s(u)$, equaling one indicates that TN_j emits E_e molecules of the m-th type at the instant of $t = uT_s$, where $m = 1, \cdots, M$ and $j = 1, \cdots, M$.

The RX observes the number of molecules of M types within each RN to detect the transmitted symbol. Assume that a Genie-aided ML (GML) detector has the access to the ideal knowledge of the previous L symbols. The u-th estimated space symbol $\hat{\mathbf{X}}_u^s$ can be detected as

$$\begin{aligned}\hat{\mathbf{X}}_u^s &= \arg\max_{\tilde{\mathbf{S}}_u^s \in \mathbf{S}^s} \prod_{m=1}^{M} \prod_{i=j=1}^{M} \Pr\left(Z_{m,i}(u) = z_{m,i}(u) | \tilde{s}_{m,j}^s(u)\right) \\ &= \arg\max_{\tilde{\mathbf{S}}_u^s \in \mathbf{S}^s} \sum_{m=1}^{M} \sum_{i=j=1}^{M} \ln\left(\Pr\left(Z_{m,i}(u) = z_{m,i}(u) | \tilde{s}_{m,j}^s(u)\right)\right),\end{aligned} \tag{4}$$

where the conditional probability mass function (PMF) of $Z_{m,i}(u)$ is given by

$$\Pr(Z_{m,i}(u) = z_{m,i}(u) | s_{m,j}^s(u)) = \frac{[\Lambda_{m,i}(u)]^{z_{m,i}(u)} e^{-\Lambda_{m,i}(u)}}{z_{m,i}(u)}, \tag{5}$$

where $\Lambda_{m,i}(u)$ is given by (3). After substituting (5) into (4), and removing the common terms, the GML detector can be simplified to

$$\hat{\mathbf{X}}_u^s = \arg\max_{\tilde{\mathbf{S}}_u^s \in \mathbf{S}^s} \sum_{m=1}^{M} \sum_{i=j=1}^{M} z_{m,i}(u) \ln\left(\Lambda_{m,i}\left(u | \tilde{s}_{m,j}^s(u)\right)\right). \tag{6}$$

However, due to the limited computational capacity of nanomachine transceivers, the GML detection is not realistic. Motivated by the fact that it is difficult to obtain the information of previously emitted symbols and CIR, we consider a low-complexity ML (LML) detection method, which determines the transmitted symbol by the number of molecules obtained in the current symbol. In this case, the Poisson parameter in (3) can be rewritten as

$$\begin{aligned}\Lambda_{m,i}(u) =& E_e V_r \sum_{j=1}^{M} \Bigg(s_{m,j}^s(u) h_{ij}[0] \\ &+ \sum_{\alpha=u-L}^{u-1} s_{m,j}^s(\alpha) h_{ij}[u-\alpha] \Bigg) + \lambda_{env} \\ =& \sum_{j=1}^{M} s_{m,j}^s(u) \lambda_{ij,0} + \Lambda_c + \lambda_{env},\end{aligned} \tag{7}$$

where Λ_c is the average effect from L previously transmitted symbols. Based on (6) and (7), the LML detector can be presented as

$$\begin{aligned}\hat{\mathbf{X}}_u^s &\overset{(a)}{=} \arg\max_{\tilde{\mathbf{S}}_u^s \in \mathbf{S}^s} \sum_{m=1}^{M} \sum_{i=j=1}^{M} z_{m,i}(u) \ln\left(\tilde{s}_{m,j}^s(u) \lambda_{ij,0} + \lambda_{env}\right) \\ &\overset{(b)}{=} \arg\max_{\tilde{\mathbf{S}}_u^s \in \mathbf{S}^s} \sum_{m=1}^{M} \sum_{i=j=1}^{M} z_{m,i}(u) \tilde{s}_{m,j}^s(u),\end{aligned} \tag{8}$$

where (a) holds since Λ_c is a constant term regardless of activation patterns. The reason behind this result is that each TN and also each type are always activated once within a symbol period in MTPSK-SD.[1] Equation (b) holds when the Poisson parameter λ_{env} resulted from the environment noise is negligible in comparison with $\lambda_{ij,0}$.

After obtaining $\hat{\mathbf{X}}_u^s$, the RX maps $\hat{\mathbf{X}}_u^s$ to the corresponding bit sequence according to the coding rule to be presented in subsection III-A-3.

2) TI-MTPSK-SD: In MTPSK-SD, different TNs emit different types of molecules at the same time; however, due to ILI, each RN samples non-zero molecules of M types, which seriously deteriorates the detection performance. In order to reduce ILI, especially when the separation distance d_{RN} of RNs is small in comparison to the radius r of RN, we propose the TI-MTPSK-SD, whose principle is described below.

In TI-MTPSK-SD, TX controls M TNs to release molecules at M different instants within a symbol duration T_s. RNs synchronize with their corresponding TNs to sample at different timings with the maximum concentration. Therefore, compared with MTPSK-SD, the only additional parameter required by TI-MTPSK-SD is the interleaving offset interval, denoted by T_{TI}, which can be optimized by aiming at minimizing the ILI in the intended link. However, the optimum value may vary according to different system parameters, such as d and d_{RN}. For simplicity, we set $T_{TI} = T_s/M$, and assume that all the later proposed modulation schemes have an equal emission interval $T_e = T_s/M$ within a symbol duration of T_s. Moreover, at each emission instant, the TN to be activated is the one that is farthest from the previously activated TN and non-activated within the current symbol duration. This activating strategy aims at further increasing the emission intervals between the adjacent TNs to reduce ILI.

[1]For the other modulation schemes to be proposed, since each type is only activated once per symbol period, and each TN and emission instant have an equal activation possibility, (a) of (8) maintains valid.

TABLE I
MAPPING TABLE OF COMPLEMENTARY CODING SCHEME FOR $M = 4$

Permutation	Bit Sequence	Opposite Permutation	Bit Sequence
{1, 2, 3, 4}	[0, 0, 0, 0]	{3, 4, 1, 2}	[1, 1, 1, 1]
{1, 2, 4, 3}	[0, 0, 0, 1]	{3, 4, 2, 1}	[1, 1, 1, 0]
{1, 4, 3, 2}	[0, 0, 1, 0]	{3, 2, 1, 4}	[1, 1, 0, 1]
{1, 4, 2, 3}	[0, 0, 1, 1]	{3, 2, 4, 1}	[1, 1, 0, 0]
{1, 3, 4, 2}	[0, 1, 0, 0]	{3, 1, 2, 4}	[1, 0, 1, 1]
{1, 3, 2, 4}	[0, 1, 0, 1]	{3, 1, 4, 2}	[1, 0, 1, 0]
{2, 4, 3, 1}	[0, 1, 1, 0]	{4, 2, 1, 3}	[1, 0, 0, 1]
{2, 4, 1, 3}	[0, 1, 1, 1]	{4, 2, 3, 1}	[1, 0, 0, 0]

To clearly explain the merit of TI-MTPSK-SD, we compare the transmit matrix of TI-MTPSK-SD with that of MTPSK-SD. Let us define $\mathbf{H}_{MT}[0]$ as the transmit matrix of MTPSK-SD for the current symbol, which can be represented as

$$\mathbf{H}_{MT}[0] = \begin{bmatrix} h_{1,1}[0] & \cdots & h_{1,j}[0] & \cdots & h_{1,M}[0] \\ \vdots & & \vdots & & \vdots \\ h_{i,1}[0] & \cdots & h_{i,j}[0] & \cdots & h_{i,M}[0] \\ \vdots & & \vdots & & \vdots \\ h_{M,1}[0] & \cdots & h_{M,j}[0] & \cdots & h_{M,M}[0] \end{bmatrix}, \quad (9)$$

where each element is non-zero, because all TNs are activated at the same time. By contrast, for TI-MTPSK-SD, since RN_i will not be influenced by the molecules emitted after the i-th instant, the transmit matrix $\mathbf{H}_{TI}[0]$ of TI-MTPSK-SD can be arranged as a lower triangular matrix, i.e.,

$$\mathbf{H}_{TI}[0] = \begin{bmatrix} h_{1,1}[0] & & & 0 \\ h_{2,1}\left[\frac{1}{M}\right] & h_{2,2}[0] & & \\ \vdots & \vdots & \ddots & \\ h_{M,1}\left[\frac{M-1}{M}\right] & h_{M,2}\left[\frac{M-2}{M}\right] & \cdots & h_{M,M}[0] \end{bmatrix}, \quad (10)$$

where half of the non-diagonal elements are zero elements, meaning a significant ILI reduction. The reason behind this is that TN_j does not interfere RN_i, provided that $j > i$ [40].

3) Complementary Coding: As shown in (8), the estimated symbol is impaired by ILI. Therefore, we present a selection rule of activation patterns and a complementary coding scheme in the sequel, which can combat this interference. Here the basic idea is to avoid activating the permutations that are prone to ILI, and to reduce the BER caused by the symbol error detection. First, we introduce the selection principle of the activation patterns based on the fact that ILI is dominated by adjacent links. This phenomenon means that a permutation candidate is least likely to be erroneously detected as its opposite permutation. In the opposite permutation, each type of molecules is emitted by the the farthest TN from the activated TN in the original permutation. For example, if TN_1 is activated to transmit molecules of the first type in the original permutation, RN_3 is expected to receive the least molecules of this type. Therefore, TN_3 is arranged to emit molecules of the first type in the opposite permutation.

For ease of understanding, an example for $M = 4$ is presented in Table I. Since $4! > 2^{\lfloor \log_2 4! \rfloor}$, 8 out of 24 permutations are selectively discarded. These 8 permutations can be arbitrary four pairs of complementary permutations so that the reserved permutations constitute opposite permutations in the mapping table. Then, the complementary coding scheme is designed based on the following two rules: a) Let each pair of complementary bit sequences be mapped to the complementary permutations that have the lowest probability of detection-error. The complementary bit sequences refer to the two bit sequences where two corresponding bits have the opposite values of 0 or 1, as shown by $[0, 0, 0, 0]$ and $[1, 1, 1, 1]$ in Table I. b) The two bit sequences, which correspond to the two permutations prone to the transposition error resulted from adjacent TNs, have the least number of different bits or the smallest Hamming distance, as shown in the Rows 1 and 2 of Table I for the permutations of $\{1, 2, 3, 4\}$ and $\{1, 2, 4, 3\}$.

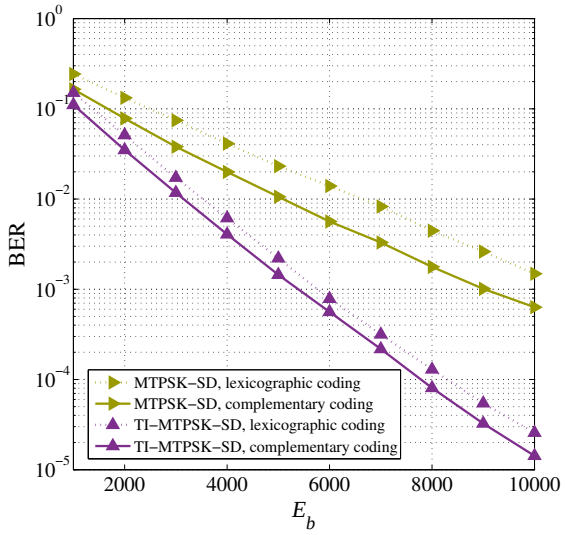

Fig. 2. Comparison between MTPSK-SD and TI-MTPSK-SD with complementary coding and lexicographic ordering coding in terms of BER with parameters chosen as: $M = 4$, $d = 25\mu$m, $d_{RN} = 10\mu$m, $r = 5\mu$m, $D = 2.2 \times 10^{-9}\mathrm{m}^2/\mathrm{s}$, and $c = 10$bit/s.

Figure 2 compares the BER performance of MTPSK-SD and TI-MTPSK-SD employing the proposed complementary coding with their counterparts employing the lexicographic ordering coding presented in [41, 42]. For a fair comparison, the BER is evaluated versus the emitted number of molecules per bit E_b in a 4×4 MIMO system with $d = 25\mu$m, $d_{RN} = 10\mu$m, $r = 5\mu$m, $D = 2.2 \times 10^{-9}\mathrm{m}^2/\mathrm{s}$, data rate $c = 10$bit/s, and $\lambda_{env} = 0.0001$. As shown in Fig. 2, the gap between the two modulation schemes with complementary coding and those with lexicographic ordering coding enlarges as E_b increases, where complementary coding can save up to 1000 and 2000 molecules per bit for TI-MTPSK-SD and MTPSK-SD, respectively. It is worth noting that the complementary coding can be employed in any modulation scheme that contains the MTPSK-SD part under the symmetrical MIMO topology, including our spatio-temporal modulation schemes to be introduced in the next subsection.

B. Spatio-Temporal Modulation Schemes

1) MTPSK-SD-TD: Inspired by the TI-MTPSK-SD, where different TNs can emit molecules of different types at different

instants instead of at the same time, we combine MTPSK-SD with MTPSK-TD [27] to propose a new modulation method, termed as MTPSK-SD-TD. MTPSK-SD-TD not only inherits the anti-ISI characteristic of MTPSK-TD, but also remains the ILI-combating ability inherited from TI-MTPSK-SD.

To implement MTPSK-SD-TD, we assume that the u-th symbol can potentially transmit b information bits, which can be divided into two parts for different purposes: The first part, termed as space bits and consisting of b_1 bits, determines the order of the M types to be employed by M individual TNs; the second part, named time bits and comprised of b_2 bits, selects M different emission instants for M different molecular types. Note that the M emission instants have equal time intervals within a symbol duration T_s. The order set of types forms two full permutations on individual TNs and different emission instants respectively, such that $b_1 = b_2 = \lfloor \log_2 M! \rfloor$.

We choose $N = 2^{b_1}$ out of the $M!$ permutations of types employed by individual TNs to form a space symbol set $\mathbf{S}^s$, which has the same items as $\mathbf{S}$ in MTPSK-SD. The (m, j)-th entry of $\mathbf{S}^s_u$, denoted by $s^s_{m,j}(u)$, equaling one indicates that TN_j emits molecules of the m-th type within the u-th symbol. Then the time symbol set $\mathbf{S}^t = \left\{\mathbf{S}^t_1, \mathbf{S}^t_2, \cdots, \mathbf{S}^t_N\right\}$ is determined by selecting N out of the $M!$ permutations of types activated at different instants. The (m, v)-th entry of $\mathbf{S}^t_u$, denoted by $s^t_{m,v}(u)$, equaling one means that the molecules of the m-th type are emitted at the v-th instant within the u-th symbol, where $v = 1, \cdots, M$.

At the receiver end, MTPSK-SD-TD can achieve the optimal detection performance via the ML detection that decodes the space and time symbols jointly. Considering that RX has no access to CIR information or the previously transmitted symbols, the optimal ML detection based on (8) can be formulated as

$$\left\langle \hat{\mathbf{X}}^s_u, \hat{\mathbf{X}}^t_u \right\rangle = \arg \max_{\tilde{\mathbf{s}}^s_u \in \mathbf{S}^s, \tilde{\mathbf{s}}^t_u \in \mathbf{S}^t} \sum_{v=1}^{M} \sum_{m=1}^{M} \sum_{i=j=1}^{M} z_{m,i}(v) \tilde{s}^s_{m,j}(u) \, \tilde{s}^t_{m,v}(u), \quad (11)$$

where $z_{m,i}(v)$ denotes the molecular number of the m-th type sampled by RN_i at the v-th instant within the u-th symbol, whose notation u is omitted for brevity; $\hat{\mathbf{X}}^s_u$ and $\hat{\mathbf{X}}^t_u$ are the estimated space symbol and time symbol, respectively.

However, (11) indicates that the optimal detector has a search complexity of $\mathcal{O}(N^2)$, which may be a heavy task for nanomachines with the constraints on size and computing capability, especially for a large N. Therefore, we propose two low-complexity detection methods for the MTPSK-SD-TD employed in MIMO MCvD systems, namely the time-based and space-based LML detectors.

The time-based LML detector first detects the time symbol by summing up the number of received molecules over all RNs according to different types, and then determines the space symbol based on the estimated emission instants. Due to the nature of UCA that the molecules received by each RN undergo the channel with symmetric coefficients, the maximum ratio combining (MRC) is equivalent to equal gain combining (EGC) for the considered system topology [30]. Therefore, we choose EGC as the combining method in this paper to avoid additional overhead when computing the weighting coefficients of MRC. The total number of the molecules of the m-th type received by all RNs at the v-th instant can be expressed as

$$z_{m,v} = \sum_{i=1}^{M} z_{m,i}(v). \quad (12)$$

Based on (12), the RX detects the time symbol by performing

$$\hat{\mathbf{X}}^t_u = \arg \max_{\tilde{\mathbf{s}}^t_u \in \mathbf{S}^t} \sum_{v=1}^{M} \sum_{m=1}^{M} z_{m,v} \tilde{s}^t_{m,v}(u). \quad (13)$$

According to the estimated time symbol of $\hat{\mathbf{X}}^t_u$, the number of received molecules of each type that corresponds to the estimated emission instants is chosen from all the numbers of molecules observed within the u-th symbol, which can be represented as

$$z_{m,i} = z_{m,i}(v), \quad for \ (m, v) \in \hat{\mathbf{X}}^t_u. \quad (14)$$

By using (14), the space symbol can be detected as

$$\hat{\mathbf{X}}^s_u = \arg \max_{\tilde{\mathbf{s}}^s_u \in \mathbf{S}^s} \sum_{m=1}^{M} \sum_{i=j=1}^{M} z_{m,i} \tilde{s}^s_{m,j}(u). \quad (15)$$

The space-based LML detector estimates the space symbol before detecting the time symbol. For molecules of each type, every RN sums up the M individual samples within the current symbol. To be precise, the sum of numbers of the m-th type molecules received by RN_i at all instants can be formulated as

$$z_{m,i} = \sum_{v=1}^{M} z_{m,i}(v), \quad (16)$$

where we assume that samples at different instants are added with equaling weights to restrict the computational complexity of the detector and facilitate its implementation for MC. The space symbol is detected by substituting (16) into (15). The estimated space symbol can determine the activated TN_j and its corresponding molecular type. Based on $\hat{\mathbf{X}}^s_u$, we select the number of received molecules of the m-th type transmitted by the estimated TN from all the $\{z_{m,i}(v)\}$ sampled in the current symbol as follows

$$z_{m,v} = z_{m,i}(v), \quad for \ (m, j) \in \hat{\mathbf{X}}^s_u, \ i = j. \quad (17)$$

Then, according to (17) the time symbol can be obtained in the same way as (13).

Note that the difference between the above two low-complexity detectors is not just the detection order. The array gain, which is detailed in [20], achieved by the EGC in the time-based LML detector is more than the gain brought by the combining method in the space-based LML detector. However, this superiority of the time-based LML detector will be exhausted when ISI is serious but ILI is minor, which means that there exists a trade-off between ISI-combating ability and ILI-combating ability for the proposed detectors.

Figure 3 shows this trade-off by comparing the BERs of MTPSK-SD-TD with respectively the time-based LML detector and the space-based LML detector in ILI-dominant and

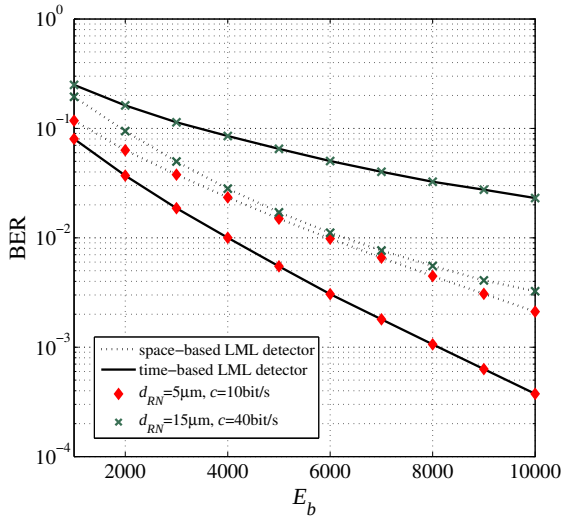

Fig. 3. Comparison between MTPSK-SD-TD with time-based LML detector and space-based LML detector in terms of BER with parameters chosen as: $d_{RN} = 5\mu$m, $c = 10$bit/s; $d_{RN} = 15\mu$m, $c = 40$bit/s.

ISI-dominant scenarios, where $d_{RN} = 5\mu$m, $c = 10$bit/s and $d_{RN} = 15\mu$m, $c = 40$bit/s (other parameters are chosen the same as those in Fig. 2). The simulation results demonstrate that the time-based LML detector outperforms the space-based LML detector when ILI is dominant, but underperforms the space-based counterpart when the effect of ISI predominates.

2) MTPSK-TD-SSK: The proposed MTPSK-SD-TD can mitigate the impacts of ISI and ILI at the same time. Consider the case that the transceiver can communicate at a high data rate, when there is enough space to separate TNs and RNs on TX and RX, respectively. In this case, the effect of ISI is more serious than that of ILI, and hence a modulation method that can efficiently combat ISI is desirable. To this objective, MTPSK-TD-SSK is proposed, as described below.

MTPSK-TD-SSK is designed based on the SSK employed in the space domain [29] and the MTPSK-TD [27]. The information bits are separated into space bits and time bits comprised of b_1 and b_2 bits, respectively. The space bits choose a TN to activate for each molecular type. It is worth noting that the activated TNs can be the same for different molecular types, which means that the process of selecting the TN from M TN candidates is performed by M types of molecules. Thus, in total $b_1 = M\log_2 M$ space bits can be conveyed per symbol. The time bits determine the permutation order of the M types transmitted at M different emission instants of a symbol, which can hence deliver $b_2 = \lfloor \log_2 M! \rfloor$ time bits per symbol. It is noteworthy that the numbers of molecule types, TNs and RNs, and emission instants within the symbol are restricted to be the same throughout the paper to facilitate the comparison of different modulation schemes.

Since the TNs activated by different molecular types are independent, the space symbol can be determined one by one according to molecular types. Let us take the m-th type for demonstration to formulate the space symbol set denoted as $\mathbf{s}_m^s = \left\{\mathbf{s}_{m,1}^s, \cdots, \mathbf{s}_{m,j}^s, \cdots, \mathbf{s}_{m,M}^s\right\}$. In the space symbol vector $\mathbf{s}_{m,j}^s$, only the j-th term $s_{m,j}^s$ equals one, while others equal zero, which represents that the m-th type of molecules are transmitted by TN_j. The principle to transmit the time symbol is the same as that in the proposed MTPSK-TD-SD.

Similar to the time-based LML detector of MTPSK-SD-TD, the detector of MTPSK-TD-SSK can first detect the time symbol $\hat{\mathbf{X}}_u^t$ based on the EGC method in (12) and the detection criterion in (13). Then, according to the output $\hat{\mathbf{X}}_u^t$, the number of molecules of each type observed at the corresponding instant is chosen based on (14). The space symbols conveyed by the M types are detected one by one, where the detection rule for the m-th type can be expressed as

$$\hat{\mathbf{x}}_m^s = \arg \max_{\tilde{\mathbf{s}}_{m,j}^s \in \mathbf{s}_m^s, i=j} z_{m,i} \tilde{s}_{m,j}^s. \tag{18}$$

The detector can partially restore b_1 bits based on $\hat{\mathbf{x}}_m^s$ immediately, without waiting for the others. In order to facilitate performance analysis, we use the M estimated $\{\hat{\mathbf{x}}_m^s\}$ to form a matrix $\hat{\mathbf{X}}_u^s$, the m-th row of which is $\hat{\mathbf{x}}_m^s$.

3) MTPSK-SD-PPM: The above MTPSK-TD-SSK is designed to mitigate ISI in the Molecular MIMO systems with a relatively large d_{RN}. This scheme may not work well in the scenario where TNs and/or RNs are not separated with sufficient distance, due to the limited spaces of transmitter and/or receiver. For this sake, we propose MTPSK-SD-PPM to simultaneously combat ILI while reducing ISI.

Combining MTPSK-SD with PPM [26], MTPSK-SD-PPM encodes information bits by first executing the permutation in the space domain, so that each of the M TNs activates one type of molecules. This process conveys $b_1 = \lfloor \log_2 M! \rfloor$ space bits. Then for each of the M TNs, one of the M time instants of a symbol is selected to transmit the correspondingly activated type of molecules. As there are M TNs, in total $b_2 = M\log_2 M$ time bits can be delivered.

It can be shown that the space symbol set $\mathbf{S}^s$ in MTPSK-SD-PPM is the same as that in MTPSK-SD-TD. Since the activated instants of different molecular types are independent, the emission instants for different types can be the same, which is different from the design criterion of the time symbol in MTPSK-SD-TD. Due to the independence of the activated time instants among M molecular types, we focus on the m-th type for analysis to form, which has a symbol set $\mathbf{s}_m^t = \left\{\mathbf{s}_{m,1}^t, \cdots, \mathbf{s}_{m,v}^t, \cdots, \mathbf{s}_{m,M}^t\right\}$, where only the v-th entry $s_{m,v}^t$ in $\mathbf{s}_{m,v}^t$ equals one, indicating that the m-th type of molecules is transmitted only at the v-th instant.

At the receiver end, the time symbol is detected first. After obtaining $\{z_{m,v}\}$, the transmitted time symbol for the m-th type can be estimated with the aid of the EGC method by performing

$$\hat{\mathbf{x}}_m^t = \arg \max_{\tilde{\mathbf{s}}_{m,v}^t \in \mathbf{s}_m^t} z_{m,v} \tilde{s}_{m,v}^t. \tag{19}$$

The M detected $\left\{\hat{\mathbf{x}}_m^t\right\}$ are then combined to form the matrix $\hat{\mathbf{X}}_u^t$, whose m-th row is $\hat{\mathbf{x}}_m^t$. Then based on the estimated $\hat{\mathbf{X}}_u^t$ and (14), we choose the numbers of molecules of different types sampled at the corresponding instants to obtain $z_{m,i}$. The space symbol $\hat{\mathbf{X}}_u^s$ can be detected by substituting $z_{m,i}$ into the detection method given in (15).

IV. Performance Analysis

In this section, we derive the BER upper bound of the MTPSK-SD-TD, when assuming the time-based LML detector, which detects the time symbol before the space symbol. The analysis for the MTPSK-SD, TI-MTPSK-SD, MTPSK-TD-SSK, and MTPSK-SD-PPM can be performed similarly, and thus is omitted for brevity.

Let us first consider the time symbol $\mathbf{X}_u^t$ and define $\Pr\left(\mathbf{S}_k^t \to \mathbf{S}_l^t\right)$ as the unconditional pairwise error probability (PEP) of transmitting $\mathbf{S}_k^t$ and deciding on $\mathbf{S}_l^t$, where $l \neq k$. According to the union bounding technique, the BER of time symbol can be upper bounded by

$$P_b^t \leq \frac{1}{N}\sum_{k=1}^{N}\sum_{l=1}^{N}\Pr\left(\mathbf{S}_k^t \to \mathbf{S}_l^t\right)\frac{e\left(\mathbf{S}_k^t \to \mathbf{S}_l^t\right)}{b_2}, \tag{20}$$

where $e\left(\mathbf{S}_k^t \to \mathbf{S}_l^t\right)$ denotes the number of error bits corresponding to the pairwise error event.

Since the detection of current time symbol $\mathbf{X}_u^t$ is affected by the previously transmitted L symbols, denoted by $\left\langle \mathbf{X}_u^t, \mathbf{X}_u^s \right\rangle^L$, the unconditional PEP can be expressed as

$$\Pr\left(\mathbf{S}_k^t \to \mathbf{S}_l^t\right) = \frac{1}{N_{\left\langle \mathbf{X}_u^t, \mathbf{X}_u^s \right\rangle^L \in \left\langle \mathbf{S}^t, \mathbf{S}^s \right\rangle^L}^{2L}} \sum \Pr\left(\mathbf{S}_k^t \to \mathbf{S}_l^t | \left\langle \mathbf{X}_u^t, \mathbf{X}_u^s \right\rangle^L\right). \tag{21}$$

The details on the derivation of $\Pr\left(\mathbf{S}_k^t \to \mathbf{S}_l^t | \left\langle \hat{\mathbf{X}}_u^t, \hat{\mathbf{X}}_u^s \right\rangle^L\right)$ are given in the sequel. Similar to (a) of (8), the detection criterion of $\hat{\mathbf{X}}_u^t$ shown in (13) can be rewritten as

$$\hat{\mathbf{X}}_u^t = \arg\max_{\tilde{\mathbf{S}}_u^t \in \mathbf{S}^t} \sum_{v=1}^{M}\sum_{m=1}^{M} z_{m,v} \ln\left(\tilde{s}_{m,v}^t(u)\,\Lambda_0 + M\lambda_{env}\right), \tag{22}$$

where $\Lambda_0 = \sum_{i=1}^{M} \lambda_{ij,0}$. The subscript j can be omitted, since the sum of channel coefficients for each TN is equal to each other. According to (22), the transmitted $\mathbf{S}_k^t$ is erroneously detected as $\mathbf{S}_l^t$, when

$$\begin{aligned}&\sum_{(m,v)\in\Omega_k\cup\Omega_l} z_{m,v}\ln\left(s_{m,v}^t(k)\,\Lambda_0 + M\lambda_{env}\right)\\ &\leq \sum_{(m,v)\in\Omega_k\cup\Omega_l} z_{m,v}\ln\left(s_{m,v}^t(l)\,\Lambda_0 + M\lambda_{env}\right),\end{aligned} \tag{23}$$

where $\Omega_k = \left\{(m,v)|\forall m, \forall v, s_{m,v}^t(k) = 1\right\}$. Consequently, the terms $(m,v) \in \Omega_k \cup \Omega_l$ represent that they are activated in $\mathbf{S}_k^t$ or $\mathbf{S}_l^t$. After subtracting the terms $(m,v) \in \Omega_k \cap \Omega_l$ from both sides of (23) and then re-arranging them, (23) can be simplified to

$$\begin{aligned}&\sum_{(m,v)\in\Omega_k-\Omega_l} z_{m,v}\ln\left(\frac{\Lambda_0 + M\lambda_{env}}{M\lambda_{env}}\right)\\ &-\sum_{(m,v)\in\Omega_l-\Omega_k} z_{m,v}\ln\left(\frac{\Lambda_0 + M\lambda_{env}}{M\lambda_{env}}\right) \leq 0,\end{aligned} \tag{24}$$

where the terms $(m,v) \in \Omega_k - \Omega_l$ represent that they are activated in $\mathbf{S}_k$ but inactivated in $\mathbf{S}_l$.

Since the sum of multiple independent Poisson random variables is still subject to the Poisson distribution, $z_{m,v} \sim \mathcal{P}\left(\Lambda_{m,v}\right)$, where $\Lambda_{m,v} = \sum_{i=1}^{M} \Lambda_{m,i}(v)$. Furthermore, when $\Lambda_{m,v} \gg 20$, the Poisson distribution can be approximated to a Gaussian distribution [43], i.e., $z_{m,v} \sim \mathcal{N}\left(\Lambda_{m,v}, \Lambda_{m,v}\right)$. Since the random variables in (24) are independent, the left-hand side of (24) can be expressed by a new Gaussian distributed random variable Y^t. When given the ISI symbols $\left\langle \mathbf{X}_u^t, \mathbf{X}_u^s \right\rangle^L$, the mean and variance of Y^t are given by (25) shown at the top of the next page. According to (25), the conditional PEP can be expressed as

$$\Pr\left(\mathbf{S}_k^t \to \mathbf{S}_l^t | \left\langle \mathbf{X}_u^t, \mathbf{X}_u^s \right\rangle^L\right) = Q\left(\frac{\mu_{Y^t}}{\sigma_{Y^t}}\right), \tag{26}$$

where $Q(x) = (2\pi)^{-1/2}\int_x^\infty e^{-t^2/2}dt$.

The BER performance of $\hat{\mathbf{X}}_u^s$ depends on the detection results of $\hat{\mathbf{X}}_u^t$, and the symbol error rate can be calculated by

$$P_s^t \approx \frac{1}{N}\sum_{k=1}^{N}\sum_{l=1, l\neq k}^{N}\Pr\left(\mathbf{S}_k^t \to \mathbf{S}_l^t\right). \tag{27}$$

Based on (27) and the union bounding technique, the BER of space symbol can be upper bounded by (28), shown at the top of the next page. The term $\frac{1}{2}P_s^t$ means that when the time symbol $\mathbf{S}_k^t$ is detected incorrectly, the BER of the space symbol equals 0.5. Since $\Pr\left(\mathbf{S}_k^s \to \mathbf{S}_l^s | \left\langle \mathbf{X}_u^t, \mathbf{X}_u^s \right\rangle^L\right)$ can be calculated in a similar way as $\Pr\left(\mathbf{S}_k^t \to \mathbf{S}_l^t | \left\langle \mathbf{X}_u^t, \mathbf{X}_u^s \right\rangle^L\right)$, we omit its derivation and just give the mean and variance of Y^s in (29), shown at the top of the next page, where $\lambda_0 = E_e V_r h_{ii}[0]$ and $\Lambda_{m,i} = \Lambda_{m,i}(v), for\ \ (m,v) \in\ \mathbf{S}_k^t$. Based on (20) and (28), the total BER of MTPSK-SD-TD is given by

$$P_b = \frac{b_1 P_b^s + b_2 P_b^t}{b}. \tag{30}$$

V. Numerical Results

In this section, first, the theoretical and simulation results for the BERs of MTPSK-SD, TI-MTPSK-SD, MTPSK-SD-TD, MTPSK-TD-SSK, and MTPSK-SD-PPM for MIMO MCvD systems are presented. Then we resort to a simulated study to show the envisioned BER benefits of our proposed modulation schemes in the scenarios impaired by various levels of ISI and ILI. MTPSK-SD and TI-MTPSK-SD employ the LML detector, while MTPSK-SD-TD, MTPSK-TD-SSK, and MTPSK-SD-PPM use the time-based LML detector. All of the proposed schemes adopt the complementary coding. We choose QMSSK, MSM, RC-MIMO as benchmarks, where both QMSSK and MSM employ the maximum count detector [30]; and RC-MIMO uses the threshold detector with the CIR information [20]. For a fair comparison, all schemes employ the same number of molecular types, emitted molecules per bit, data rate, numbers of TNs and RNs, and symmetrical system topology. The specific system parameters are listed in Table II. The considered ISI length L is restricted to

$$L = \arg\min_{v-\alpha}\left\{h_{ii}[v-\alpha]/h_{ii}[0] \leq 1\%\right\}. \tag{31}$$

Figure 4 shows the BER upper bounds with simulation results for MTPSK-SD, TI-MTPSK-SD, MTPSK-SD-TD, MTPSK-TD-SSK, and MTPSK-SD-PPM, when $d_{RN} = 5\mu$m and $c = 10$bit/s are considered. It is observed that the theoretical

$$\mu_{Y^t} = \sum_{(m,v)\in\Omega_k-\Omega_l} \Lambda_{m,v} \ln\left(\frac{\Lambda_0 + M\lambda_{env}}{M\lambda_{env}}\right) - \sum_{(m,v)\in\Omega_l-\Omega_k} \Lambda_{m,v} \ln\left(\frac{\Lambda_0 + M\lambda_{env}}{M\lambda_{env}}\right),$$
$$\sigma^2_{Y^t} = \sum_{(m,v)\in\Omega_k-\Omega_l} \Lambda_{m,v} \ln^2\left(\frac{\Lambda_0 + M\lambda_{env}}{M\lambda_{env}}\right) + \sum_{(m,v)\in\Omega_l-\Omega_k} \Lambda_{m,v} \ln^2\left(\frac{\Lambda_0 + M\lambda_{env}}{M\lambda_{env}}\right). \quad (25)$$

$$P_b^s \le \frac{1}{N}\sum_{k=1}^{N}\sum_{l=1}^{N}\left(\left(1-P_s^t\right)\Pr\left(\mathbf{S}_k^s \to \mathbf{S}_l^s\right)\frac{e\left(\mathbf{S}_k^s \to \mathbf{S}_l^s\right)}{b_1}\right) + \frac{1}{2}P_s^t$$
$$= \frac{1-P_s^t}{N^{2L+1}}\sum_{k=1}^{N}\sum_{l=1}^{N}\sum_{\langle \mathbf{X}_u^t, \mathbf{X}_u^s\rangle^L \in \langle \mathbf{S}^t, \mathbf{S}^s\rangle^L}\left(\Pr\left(\mathbf{S}_k^s \to \mathbf{S}_l^s | \langle \mathbf{X}_u^t, \mathbf{X}_u^s\rangle^L\right)\frac{e\left(\mathbf{S}_k^s \to \mathbf{S}_l^s\right)}{b_1}\right) + \frac{1}{2}P_s^t. \quad (28)$$

$$\mu_{Y^s} = \sum_{(m,i)\in\Omega_k-\Omega_l} \Lambda_{m,i} \ln\left(\frac{\lambda_0 + \lambda_{env}}{\lambda_{env}}\right) - \sum_{(m,i)\in\Omega_l-\Omega_k} \Lambda_{m,i} \ln\left(\frac{\lambda_0 + \lambda_{env}}{\lambda_{env}}\right),$$
$$\sigma^2_{Y^s} = \sum_{(m,i)\in\Omega_k-\Omega_l} \Lambda_{m,i} \ln^2\left(\frac{\lambda_0 + \lambda_{env}}{\lambda_{env}}\right) + \sum_{(m,i)\in\Omega_l-\Omega_k} \Lambda_{m,i} \ln^2\left(\frac{\lambda_0 + \lambda_{env}}{\lambda_{env}}\right). \quad (29)$$

TABLE II
SYSTEM PARAMETERS

Parameter	Variable	Value
Types of molecules	M	4
Radius of RN	r	5 μm
Distance of paired link	d	25 μm
Diffusion coefficient	D	2.2×10^{-9} m^2/s
Emitted molecules per bit	E_b	$[1000, 10000]$
Number of TNs and RNs	M	4
Data rate	c	$[5, 40]$ bit/s
Separation distance of RNs	d_{RN}	$[1, 10]$ μm
Mean of environment noise	λ_{env}	0.0001
Length of ISI	L	$[2, 28]$

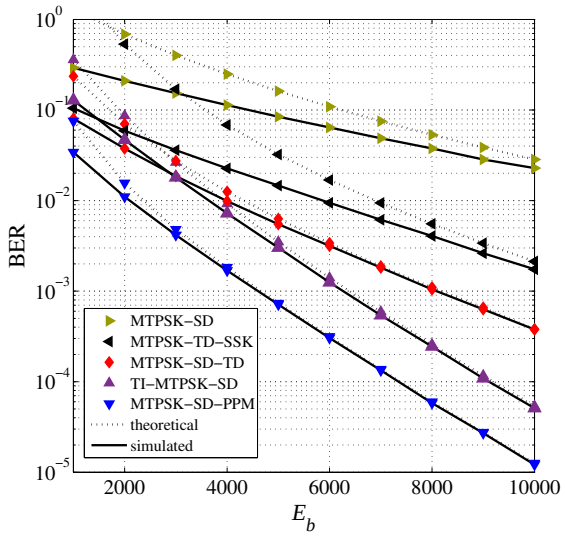

Fig. 4. BER upper bounds for MTPSK-SD, TI-MTPSK-SD, MTPSK-SD-PPM, MTPSK-TD-SSK, and MTPSK-SD-TD with parameters chosen as: $d_{RN} = 5\mu$m and $c = 10$bit/s.

BERs agree well with their simulated counterparts, especially when the BER is lower than 10^{-2}. The relatively large gap between analytical and simulated BERs of MTPSK-SD can be understood by two facts: The union-bounding technique repeatedly counts the symbol error probability, whose impairment will be aggravated in the lower BER region; since MTPSK-SD cannot ensure that different TNs emit molecules at different instants, its detection performance is prone to ILI, especially when the separation distance of RNs is only 5μm, equal to the radii of RNs. Compared with MTPSK-SD, TI-MTPSK-SD significantly enhances the BER performance in the whole E_b region, which demonstrates its desirable capability of ILI mitigation at no cost of external computation or hardware complexity.

Figure 5 compares the BER simulation curves of TI-MTPSK-SD, MTPSK-SD-TD, MTPSK-TD-SSK, MTPSK-SD-PPM, RC-MIMO, QMSSK, and MSM, when $E_b = 10000$, $d_{RN} = 5\mu$m and various data rates c are considered. The chosen parameter $d_{RN} = 5\mu$m and increasing data rate c represent the communication scenarios affected by serious ILI and slight to severe ISI. As shown in Fig. 5, the BER curves of all schemes increase with the increase of c, which demonstrates that ISI always has adverse effect on the considered MIMO MCvD systems. To be precise, MTPSK-SD-PPM maintains the optimal performance within the considered data rate region. The reason behind this is twofold: Before detecting the time symbol, the employed EGC method enhances the strength of the intended signal through combining the molecules sampled by other RNs; since the number of transmitted bits per symbol of MTPSK-SD-PPM is the largest among those of compared modulation schemes, MTPSK-SD-PPM has the longest symbol duration that mitigates the effect of ISI. MSM shows a similar but underperformed performance to MTPSK-SD-PPM. This is because MSM can reduce ILI by helping channel clean itself from other types of molecules, but employing the M types to encode only $\log_2 M$ bits renders it

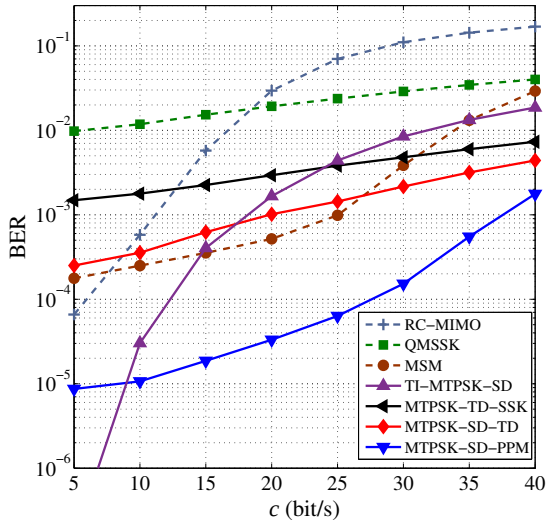

Fig. 5. BER comparison between TI-MTPSK-SD, MTPSK-SD-PPM, MTPSK-TD-SSK, MTPSK-SD-TD, QMSSK, MSM, and RC-MIMO for $E_b = 10000$, $d_{RN} = 5\mu$m, and different data rates c.

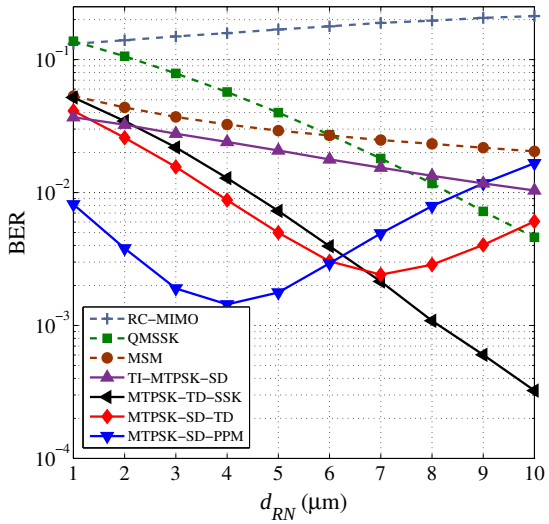

Fig. 6. BER comparison between TI-MTPSK-SD, MTPSK-SD-PPM, MTPSK-TD-SSK, MTPSK-SD-TD, QMSSK, MSM, and RC-MIMO for $E_b = 10000$, $c = 40$bit/s and different separation distances d_{RN}.

to suffer from severer ISI.

Furthermore, we observe that TI-MTPSK-SD performs the best when $c < 8$ bit/s. This can be understood since the detrimental effect of ILI is effectively suppressed by emitting molecules of different types at different instants. However, as shown in the region $c > 8$ bit/s, its performance is deteriorated rapidly as the data rate increases. The reason behind this is that the emitting and sampling instants of transceivers are interleaved to mitigate the ILI; however, since the emission interval of the same molecular type is also potentially decreased during the continuous symbol transmission, the impairment of ISI is aggravated. Compared to TI-MTPSK-SD, RC-MIMO presents a similar but underperformed performance. This is because RC exploits the constructive effect of ILI, but reduces the data rate per symbol so that RC-MIMO is more prone to ISI. Finally, we observe that the BER curves of MTPSK-SD-TD, MTPSK-TD-SSK are relatively stable, which demonstrates that both of them can combat the increasing ISI. Moreover, MTPSK-SD-TD and MTPSK-TD-SSK outperform QMSSK, since both MTPSK-SD-TD and MTPSK-TD-SSK emit molecules at different instants to partly mitigate the effect of ILI.

In MCvD MIMO systems, ILI can be mitigated by increasing the separation distances. Therefore, to show the effect of increasing ILI and serious ISI, Fig. 6 illustrates the BER comparison results for TI-MTPSK-SD, MTPSK-SD-TD, MTPSK-TD-SSK, MTPSK-SD-PPM, RC-MIMO, QMSSK, and MSM, where $E_b = 10000$, $c = 40$bit/s and different separation distances d_{RN} are assumed. From Fig. 6, we observe that the BERs of MTPSK-SD-PPM and MTPSK-SD-TD decrease first and then rise with the increase of d_{RN}. The reason behind this is that, in MTPSK-SD-PPM and MTPSK-SD-TD schemes, ILI has detrimental effect on space bits, but it has constructive effect on time bits due to the EGC gain. Furthermore, the optimal performance point of MTPSK-SD-PPM appears at $d_{RN} = 4\mu$m earlier than $d_{RN} = 7\mu$m of MTPSK-SD-TD. This is because the proportion of time bits in total information bits of MTPSK-SD-PPM is larger than the proportion of MTPSK-SD-TD. The performance of MTPSK-TD-SSK overtakes that of MTPSK-SD-PPM and MTPSK-SD-TD when $d_{RN} > 7\mu$m. This can be understood since a larger d_{RN} means a shrinking array gain of EGC for MTPSK-SD-PPM and MTPSK-SD-TD and a weaker impairment caused by ILI for space bit that is the dominant part for MTPSK-TD-SSK. Therefore, MTPSK-TD-SSK is more suitable in ILI-limited scenarios. Finally, we observe poor BER performance of TI-MTPSK-SD, QMSSK, MSM, and RC-MIMO under different values of d_{RN}, since they cannot combat the serious ISI.

Comparing Figs. 5 and 6, we observe that in communication scenarios affected by different levels of ISI and ILI, any of the four proposed extended modulation schemes can be the optimal one potentially in terms of BER performance. Therefore, when the system parameters are available and stable, we can choose the most suitable modulation scheme; otherwise, MTPSK-SD-TD can be implemented due to its stable BER performance.

VI. Conclusion

In this paper, we have proposed a molecular type permutation modulation scheme in the space domain, called MTPSK-SD, for MIMO MCvD systems, and extended it to a time interleaving version, named TI-MTPSK-SD, which can reduce ILI effectively at no cost of computation complexity. A complementary coding scheme for the symmetrical system topology has been proved to be a feasible solution for ILI mitigation. Three spatio-temporal modulation schemes, which target to different levels of ISI and ILI, have also been proposed to attain a desirable BER performance under different data rates and separation distances of receive nanomachines. When ISI or ILI is the dominant interference, the time-based LML detector and space-based LML detector have been proposed to combat ISI or ILI, respectively. BER performance analysis and simulation results have been conducted, showing that the proposed

modulation schemes with the low-complexity detector and the complementary coding rule outperform QMSSK, MSM, and RC-MIMO under various levels of ISI and ILI.

Finally, since our main objective is to construct a comprehensive spatio-temporal MTPSK system, potential issues, such as generalizing the number of molecular types and offsetting the misalignments between centers of transceivers, will be considered in our future work.

REFERENCES

[1] V. Chamola, V. Hassija, V. Gupta, and M. Guizani, "A comprehensive review of the COVID-19 pandemic and the role of IoT, drones, AI, blockchain, and 5G in managing its impact," *IEEE Access*, vol. 8, pp. 90225–90265, 2020,

[2] M. Khalid, O. Amin, S. Ahmed, B. Shihada and, M. Alouini, "Modeling of Viral Aerosol Transmission and Detection," *IEEE Trans. Commun.,* vol. 68, no. 8, pp. 4859–4873, Aug. 2020.

[3] M. Khalid, O. Amin, S. Ahmed, B. Shihada, and M. Alouini, "Communication through breath: Aerosol transmission," *IEEE Commun. Mag.,* vol. 57, no. 2, pp. 33–39, Feb. 2019.

[4] Z. Ning, K. Zhang, X. Wang, L. Guo, X. Hu, J. Huang, B. Hu, and R. Y. K. Kwok, "Intelligent edge computing in Internet of vehicles: A joint computation offloading and caching solution," *IEEE Trans. Intell. Transp. Syst.,* early access, June 2020, doi: 10.1109/TITS.2020.2997832.

[5] H. Siljak, N. Ashraf, M. T. Barros, D. P. Martins, B. Butler, A. Farhang, N. Marchetti, and S. Balasubramaniam. (2020) "Evolving intelligent reflector surface towards 6G for public health: Application in airborne virus detection," [Online]. Available: https://arxiv.org/abs/2009.02224

[6] I. F. Akyildiz, M. Pierobon, S. Balasubramaniam, and Y. Koucheryavy, "The internet of bio-nano things," *IEEE Commun. Mag.,* vol. 53, no. 3, pp. 32–40, Mar. 2015.

[7] U. A. K. Chude-Okonkwo, R. Malekian, B. T. Maharaj, and A. V. Vasilakos, "Molecular communication and nanonetwork for targeted drug delivery: A survey," *IEEE Commun. Surveys Tut.*, vol. 19, no. 4, pp. 3046–3096, 4th Quart. 2017.

[8] L. Felicetti, M. Femminella, and G. Reali, "A molecular communications system for live detection of hyperviscosity syndrome," *IEEE Trans. Nanobiosci.*, vol. 19, no. 3, pp. 410–421, July 2020.

[9] Z. Ning, P. Dong, X. Wang et al., "Mobile edge computing enabled 5G health monitoring for internet of medical things: a decentralized game theoretic approach," *IEEE J. Sel. Areas Commun.*, early access, Dec. 2020, doi: 10.1109/JSAC.2020.3020645.

[10] N. Farsad, H. B. Yilmaz, A. Eckford, C.-B. Chae, and W. Guo, "A comprehensive survey of recent advancements in molecular communication," *IEEE Commun. Surveys Tut.*, vol. 18, no. 3, pp. 1887–1919, 3rd Quart. 2016.

[11] B. Tepekule, A. E. Pusane, H. B. Yilmaz, C.-B. Chae, and T. Tugcu, "ISI mitigation techniques in molecular communication," *IEEE Trans. Mol. Biol. Multi-Scale Commun.*, vol. 1, no. 2, pp. 202–216, June 2015.

[12] E. G. Larsson, O. Edfors, F. Tufvesson, and T. L. Marzetta, "Massive MIMO for next generation wireless systems," *IEEE Commun. Mag.*, vol. 52, no. 2, pp. 186–195, Feb. 2014.

[13] L.-S. Meng, P.-C. Yeh, K.-C. Chen, and I. F. Akyildiz, "MIMO communications based on molecular diffusion," in *Proc. IEEE Global Commun. Conf. (GLOBECOM),* Anaheim, CA, USA, Dec. 2012, pp. 5380–5385.

[14] B.-H. Koo, H. B. Yilmaz, A. Eckford, and C.-B. Chae, "Detection algorithms for molecular MIMO," in *Proc. IEEE Int. Conf. Commun. (ICC),* London, UK, June 2015, pp. 1122–1127.

[15] B.-H. Koo, C. Lee, H. B. Yilmaz, N. Farsad, A. Eckford, and C.-B. Chae, "Molecular MIMO: From theory to prototype," *IEEE J. Sel. Areas Commun.*, vol. 34, no. 3, pp. 600–614, Mar. 2016.

[16] C. Lee, B.-H. Koo, and C.-B. Chae, "Demo: In-vessel molecular MIMO communications," in *Proc. IEEE Wireless Commun. Netw. Conf. Workshops (WCNC Wkshps),* Seoul, South Korea, May 2020, pp. 1–2,

[17] Y. Huang, M. Wen, L.-L. Yang, C.-B. Chae, X. Chen, and Y. Tang, "Space shift keying for molecular communication: Theory and experiment," in *Proc. IEEE Global Commun. Conf. (GLOBECOM),* Waikoloa, HI, USA, Dec. 2019, pp. 1–6.

[18] S. M. R. Rouzegar and U. Spagnolini, "Diffusive MIMO molecular communications: Channel estimation, equalization and detection," *IEEE Trans. Commun.,* vol. 67, no. 7, pp. 4872–4884, July 2019.

[19] M. C. Gursoy, A. Celik, E. Basar, A. E. Pusane, and T. Tugcu, "Molecular index modulation with space-time equalization," *IEEE Wireless Commun. Lett.*, vol. 9, no. 5, pp. 702–705, May 2020.

[20] M. Damrath, H. B. Yilmaz, C.-B. Chae, and P. A. Hoeher, "Array gain analysis in molecular MIMO communications," *IEEE Access*, vol. 6, pp. 61091–61102, 2018.

[21] C. Wu, L. Lin, W. Guo, and H. Yan, "Signal detection for molecular MIMO communications with asymmetrical topology," *IEEE Trans. Mol., Biol. Multi-Scale Commun.*, vol. 6, no. 1, pp. 60–70, July 2020.

[22] A. Noel, K. Cheung, and R. Schober, "Improving receiver performance of diffusive molecular communication with enzymes," *IEEE Trans. NanoBiosci.*, vol. 13, no. 1, pp. 31–43, Mar. 2014.

[23] J. Suzuki, T. Nakano, and M. J. Moore, *Modeling, Methodologies and Tools for Molecular and Nano-Scale Communications.* Cham, Switzerland: Springer, 2017.

[24] X. Chen, Y. Huang, L.-L. Yang, and M. Wen, "Generalized molecularshift keying (GMoSK): Principles and performance analysis," *IEEE Trans. Mol. Biol. Multi-Scale Commun.*, vol. 6, no. 3, pp. 168–183, Dec. 2020.

[25] W. Gao, T. Mak, and L. -L. Yang, "Molecular type spread molecular shift keying for multiple-access diffusive molecular communications," *IEEE Trans Mol. Biol. Multi-Scale Commun.*, early access, Nov. 2020, doi: 10.1109/TMBMC.2020.3041182.

[26] B. C. Akdeniz, A. E. Pusane, and T. Tugcu, "Position-based modulation in molecular communications," *Nano Commun. Netw.*, vol. 16, pp. 60–68, June 2018.

[27] Y. Tang, M. Wen, X. Chen, Y. Huang, and L.-L. Yang, "Molecular type permutation shift keying for molecular communication," *IEEE Trans. Mol., Biol. Multi-Scale Commun.*, vol. 6, no. 2, pp. 160–164, Nov. 2020.

[28] L. Khaloopour, M. Mirmohseni, and M. Nasiri-Kenari, "Adaptive release duration modulation for limited molecule production and storage," *IEEE Trans Mol. Biol. Multi-Scale Commun.*, vol. 5, no. 2, pp. 139–152, Nov. 2019.

[29] Y. Huang, M. Wen, L.-L. Yang, C.-B. Chae, and F. Ji, "Spatial modulation for molecular communication," *IEEE Trans. NanoBiosci.*, vol. 18, no. 3, pp. 381–395, July 2019.

[30] M. C. Gursoy, E. Basar, A. E. Pusane, and T. Tugcu, "Index modulation for molecular communication via diffusion systems," *IEEE Trans. Commun.,* vol. 67, no. 5, pp. 3337–3350, May 2019.

[31] L. Felicetti, M. Femminella, G. Reali, T. Nakano, and A. V. Vasilakos, "TCP-like molecular communications," *IEEE J. Sel. Areas Commun.* vol. 32, no. 12, pp. 2354–2367, Dec. 2014.

[32] H. ShahMohammadian, G. G. Messier, and S. Magierowski, "Blind synchronization in diffusion-based molecular communication channels," *IEEE Commun. Lett.*, vol. 17, no. 11, pp. 2156–2159, Nov. 2013.

[33] N.-R. Kim and C.-B. Chae, "Novel modulation techniques using isomers as messenger molecules for nano communication networks via diffusion," *IEEE J. Sel. Areas Commun.*, vol. 31, no. 12, pp. 847–856, Dec. 2013.

[34] A. Noel, K. C. Cheung, and R. Schober, "Using dimensional analysis to assess scalability and accuracy in molecular communication," in *Proc. IEEE Int. Conf. Commun. (ICC),* Budapest, Hungary, June 2013, pp. 818–823.

[35] I. Llatser, A. Cabellos-Aparicio, M. Pierobon, and E. Alarcon, "Detection techniques for diffusion-based molecular communication," *IEEE J. Sel. Areas Commun.*, vol. 31, no. 12, pp. 726–734, Dec. 2013.

[36] H. C. Berg, *Random Walk in Biology*. Princeton, NJ, USA: Princeton University Press, 1993.

[37] A. Noel, K. C. Cheung, and R. Schober, "Improving receiver performance of diffusive molecular communication with enzymes," *IEEE Trans. NanoBiosci.*, vol. 13, no. 1, pp. 31–43, Mar. 2014.

[38] L. Shi and L.-L. Yang, "Error performance analysis of diffusive molecular communication systems with on-off keying modulation," *IEEE Trans. Mol., Biol. Multi-Scale Commun.*, vol. 3, no. 4, pp. 224–238, Dec. 2017.

[39] M. Pierobon and I. F. Akyildiz, "Diffusion-based noise analysis for molecular communication in nanonetworks," *IEEE Trans. Signal Process.*, vol. 59, no. 6, pp. 2532–2547, June 2011.

[40] Z. Ning et al., "Partial computation offloading and adaptive task scheduling for 5G-enabled vehicular networks," *IEEE Trans. Mobile Comput.,* early access, Sept. 2020, doi: 10.1109/TMC.2020.3025116.

[41] M. Wen, E. Başar, Q. Li, B. Zheng, and M. Zhang, "Multiple-mode orthogonal frequency division multiplexing with index modulation," *IEEE Trans. Commun.*, vol. 65, no. 9, pp. 3892–3906, Sept. 2017.

[42] X. Wang, Z. Ning, S. Guo, L. Wang, "Imitation learning enabled task scheduling for online vehicular edge computing," *IEEE Trans. Mobile Comput.,* early access, July 2020, doi: 10.1109/TMC.2020.3012509.

[43] A. Papoulis, *Probability, Random Variables, and Stochastic Processes,* 3rd ed. New York: McGraw-Hill, Inc, 1991.

Yuankun Tang (Graduate Student Member, IEEE) received the B.S. degree in communication engineering from the South China University of Technology, Guangzhou, China, in 2018. He is currently pursuing the Ph.D. degree in information and communication engineering with the South China University of Technology, Guangzhou, China. In August 2019, he was a visiting student of molecular communication with Yonsei University, Seoul, South Korea. His main research interests include molecular communications and index modulation.

Yu Huang (Graduate Student Member, IEEE) received the B.S. degree in communication engineering from the Harbin University of Science and Technology, Harbin, China, in 2016. He is currently pursuing the Ph.D. degree in information and communication engineering with the South China University of Technology, Guangzhou, China. From 2018 to 2019, he was a visiting student of molecular communication with Yonsei University, Seoul, South Korea. Since January 2020, he has been visiting Cranfield University, Bedford, U.K., for emerging communication techniques. His main research interests include molecular communications and wireless communications. He was the winner of the Data Bakeoff Competition (Molecular MIMO) at the IEEE Communication Theory Workshop held in Selfoss, Iceland, in 2019.

Chan-Byoung Chae (Fellow, IEEE) received the Ph.D. degree in ECE from The University of Texas at Austin in 2008. He was a Research Engineer with the Telecommunications R&D Center, Samsung Electronics, Suwon, South Korea, from 2001 to 2005. He was with Harvard University, Cambridge, MA, USA, from 2008 to 2009, as a Post-Doctoral Research Fellow, and Bell Labs, Alcatel-Lucent, Murray Hill, NJ, USA from 2009 to 2011, as a Member of Technical Staff. He was a member of the Wireless Networking and Communications Group (WNCG), The University of Texas at Austin. He is currently an Underwood Distinguished Professor with the School of Integrated Technology, Yonsei University, South Korea.

He was a recipient/co-recipient of the Young Engineer Award from the IEEE VTS Daniel E. Noble Fellowship Award in 2008, the IEEE ComSoc AP Outstanding Young Researcher Award in 2012, the KICS Haedong Young Scholar Award in 2013, the IEEE Signal Processing Magazine Best Paper Award in 2013, the IEIE/IEEE Joint Award for Young IT Engineer of the Year in 2014, the IEEE INFOCOM Best Demo Award in 2015, the Yonam Research Award from LG Yonam Foundation in 2016, the Award of Excellence in Leadership of 100 Leading Core Technologies for Korea 2025 from the NAEK in 2017, the National Academy of Engineering of Korea (NAEK) in 2019, the IEEE DySPAN Best Demo Award in 2018, and the IEEE/KICS JOURNAL OF COMMUNICATIONS AND NETWORKS Best Paper Award in 2018. He has been serving as an Editor for IEEE COMMUNICATIONS MAGAZINE since 2016, IEEE TRANSACTIONS ON WIRELESS COMMUNICATIONS since 2012, IEEE TRANSACTIONS ON MOLECULAR, BIOLOGICAL, AND MULTI-SCALE COMMUNICATIONS since 2015, IEEE WIRELESS COMMUNICATIONS LETTERS since 2016, and IEEE/KICS JOURNAL OF COMMUNICATIONS AND NETWORKS since 2012. He is currently an Editorin-Chief of IEEE TRANSACTIONS ON MOLECULAR, BIOLOGICAL, AND MULTI-SCALE COMMUNICATIONS and a Senior Editor of IEEE WIRELESS COMMUNICATIONS LETTERS.

Wei Duan (Member, IEEE) received the Ph.D. degree from Chonbuk National University, Jeonju, South Korea, in 2017. He is currently an associate professor with Nantong University, Nantong, China. He had participated in the World Class University Project, sponsored by the National Research Foundation of Korea Grant funded by the Korean Ministry of Education Science and Technology, as a Vice Head Researcher. He has authored more than 30 journal papers. He is currently serving as an Editor for the FRONTIERS IN COMMUNICATIONS AND NETWORKS, Guest Editor for the CHINA COMMUNICATIONS (Special Issue on New Advances in Non-Orthogonal Multiple Access), and Lead Guest Editor for the WIRELESS COMMUNICATIONS AND MOBILE COMPUTING (Special Issue on Architectures, Challenges and Opportunities within 6G Emerging Technologies). His research interests include wireless communications and non-orthogonal multiple access techniques.

Miaowen Wen (Senior Member, IEEE) received the Ph.D. degree from Peking University, Beijing, China, in 2014. From 2012 to 2013, he was a Visiting Student Research Collaborator with Princeton University, Princeton, NJ, USA. He is currently an Associate Professor with South China University of Technology, Guangzhou, China. He has published two books and more than 100 journal papers. His research interests include a variety of topics in the areas of wireless and molecular communications.

Dr. Wen was a recipient of the IEEE Asia-Pacific (AP) Outstanding Young Researcher Award in 2020, and four Best Paper Awards from the IEEE ITST'12, the IEEE ITSC'14, the IEEE ICNC'16, and the IEEE ICCT'19. He was the winner in data bakeoff competition (Molecular MIMO) at IEEE Communication Theory Workshop (CTW) 2019, Selfoss, Iceland. He served as a Guest Editor for the IEEE JOURNAL ON SELECTED AREAS IN COMMUNICATIONS and for the IEEE JOURNAL OF SELECTED TOPICS IN SIGNAL PROCESSING. Currently, he is serving as an Editor for the IEEE TRANSACTIONS ON COMMUNICATIONS, and the IEEE COMMUNICATIONS LETTERS, and a Guest Editor for the IEEE JOURNAL OF SELECTED TOPICS IN SIGNAL PROCESSING (Special Issue on Advanced Signal Processing for Local and Private 5G Networks).

Lie-Liang Yang (Fellow, IEEE) received the B.Eng. degree in communications engineering from Shanghai Tiedao University, Shanghai, China, in 1988, and the M.Eng. and Ph.D. degrees in communications and electronics from Northern (Beijing) Jiaotong University, Beijing, China, in 1991 and 1997, respectively. From June 1997 to December 1997, he was a Visiting Scientist with the Institute of Radio Engineering and Electronics, Academy of Sciences of the Czech Republic. Since December 1997, he has been with The University of Southampton, U.K., where he is currently a Professor of wireless communications with the School of Electronics and Computer Science. His research interests include wireless communications, wireless networks and signal processing for wireless communications and molecular communications, and nano-networks. He has published over 390 research articles in journals and conference proceedings, authored/coauthored three books, and also published several book chapters. He is a Fellow of IET, and was a Distinguished Lecturer of the IEEE VTS. He served as an Associate Editor to the IEEE TRANSACTION ON VEHICULAR TECHNOLOGY and JOURNAL OF COMMUNICATIONS AND NETWORKS (JCN). He is an Associate Editor to IEEE ACCESS and a Subject Editor to the ELECTRONICS LETTERS.